

Modulation of carrier type in nanocrystal-in-matrix composites by interfacial doping

Richa Sharma^{1,5}, April M. Sawvel¹, Bastian Barton¹, Angang Dong¹, Raffaella Buonsanti¹, Anna Llordes¹, Eric Schaible², Stephanus Axnanda², Zhi Liu², Jeffrey J. Urban¹, Dennis Nordlund³, Christian Kisielowski¹, Delia J. Milliron^{*1,4}

¹The Molecular Foundry, Lawrence Berkeley National Laboratory, Berkeley, CA 94720, USA

²Advanced Light Source, Lawrence Berkeley National Laboratory, Berkeley, CA 94720, USA

³Stanford Synchrotron Radiation Laboratory, P.O. Box 20450, Stanford, CA 94309, USA

⁴McKetta Department of Chemical Engineering, The University of Texas at Austin, Austin, TX 78712, USA

⁵Current location: Schlumberger-Doll Research, 1 Hampshire Street, Cambridge, MA 02139, USA

*Author to whom all correspondence should be addressed. Email: milliron@che.utexas.edu

Supplementary information

Nanoparticle synthesis

PbSe nanocrystals with rock-salt structure and average size of 7 nm and first absorption feature at 2153 nm were synthesized¹ using a modified literature procedure from PbO and TOP-Se in a noncoordinating solvent (1-octadecene).

Precursor synthesis

ChaMs were prepared at room temperature in a nitrogen atmosphere glovebox by dissolution of metal chalcogenides in anhydrous hydrazine in the presence of excess chalcogen. The Sn-S ChaM is synthesized by mixing 2 mmol of SnS and 4 mmol of S in 4 ml anhydrous hydrazine and stirring for three days. The light yellow solution formed is filtered through a 0.2 μm filter to remove any undissolved solids and dried under nitrogen flow to yield a yellow powder with the

chemical formula $(\text{N}_2\text{H}_5)_4\text{Sn}_2\text{S}_6$. The Ge-S ChaM is similarly synthesized by stirring 2 mmol of GeS with 4 mmol of S in 2 ml anhydrous hydrazine for one week. The resulting colorless solution is filtered, and dried under nitrogen to yield a white crystalline powder with the expected chemical formula $(\text{N}_2\text{H}_4)_x(\text{N}_2\text{H}_5)_4\text{Ge}_2\text{S}_6$. For ligand exchange, the ChaMs of Sn-S/Ge-S is dissolved in formamide at concentrations ~ 50 mg/ml.

The $(\text{N}_2\text{H}_4)_2\text{ZnTe}$ compound is synthesized by mixing 3 mmol of ZnTe with 3 mmol Te in 6 ml anhydrous hydrazine and stirring for three days. Addition of Te increases the solubility of ZnTe in hydrazine. The red colored solution is filtered, and dried under nitrogen. For ligand exchange $(\text{N}_2\text{H}_4)_2\text{ZnTe}$ is dissolved in ethanolamine and filtered to remove undissolved solids.

Caution! Hydrazine is highly toxic and should be handled with extreme caution to prevent exposure by inhalation or absorption through the skin.

Device fabrication

Indium is thermally evaporated using a shadow mask for the source/drain contacts of TFT devices (Figure S6). Underlying the indium is a composite of indium and gold that is used as the adhesive thin-film material to attach indium onto the SiO_2 surface. The indium/gold composite is co-deposited by two-source thermal evaporation with 10 nm film thickness of each metal. The final indium metal film is 80 nm thick at deposition rates of approximately $1\text{-}2 \text{ \AA s}^{-1}$ with base pressure of 10^{-4} Pa. The substrate stage is rotated during evaporation to ensure uniform metal film deposition. High surface energy indium exhibits dewetting on silicon substrates (as well as on metal chalcogenide films) during deposition if the composite is omitted. Such a rough film morphology severely limits the film continuity, substrate adherence and electrical conductivity.

This is overcome by using a composite indium/gold film as the adhesion layer followed by indium deposition. SEM and optical images are reported in Figure S6.

Indium is used as the electrode material due to its low melting point ($\sim 156^{\circ}\text{C}$). Thus, the nanocomposite films remain protected from uncontrolled high-temperature thermal treatment during metal evaporation. We also explored the effect of thermal annealing on device characteristics by fabricating and testing devices with physically adhered (rather than thermally evaporated) indium dots as electrodes. Device data for such devices is presented in Figure S5.

Nanocomposite Characterization

UPS measurements were performed at the Stanford Synchrotron Radiation Laboratory (SSRL) at beamline 8-1 (energy range 15-200 eV), using the 2400 l/mm grating of the TGM monochromator with 100 μm slits at 80 eV, resulting in an energy resolution below 100 meV. The photoemission spectra were collected in a UHV chamber (10 \times 10 torr base pressure), equipped with physical electronics instrument (PHI) model 10-360 hemispherical energy analyzer with a multichannel detector mounted at the magic angle (54.44) with respect to the incoming photon beam. The spectrometer was operated with a pass energy of 5 eV. All spectra, including the gold reference, were collected using a sample bias (12 V) during the measurements, to overcome the workfunction of the spectrometer as well as reducing broadening and increasing transmission at very low kinetic energies. The photoelectron take-off angle was set normal to the sample surface to maximize probing depth, and the beam footprint at this incidence was about 1 \times 2 mm (incoming photon spot size 1 \times 1 mm).

SEM imaging was carried out using a Zeiss Gemini Ultra-55 Analytical Scanning Electron Microscope, using beam energies of 2-10 kV and an In-Lens detector. Atomic force microscopy (AFM) was used to characterize the thickness and surface morphology of nanocomposite membranes transferred to SiO₂-Si wafers². The membrane thickness was ca. 8nm.

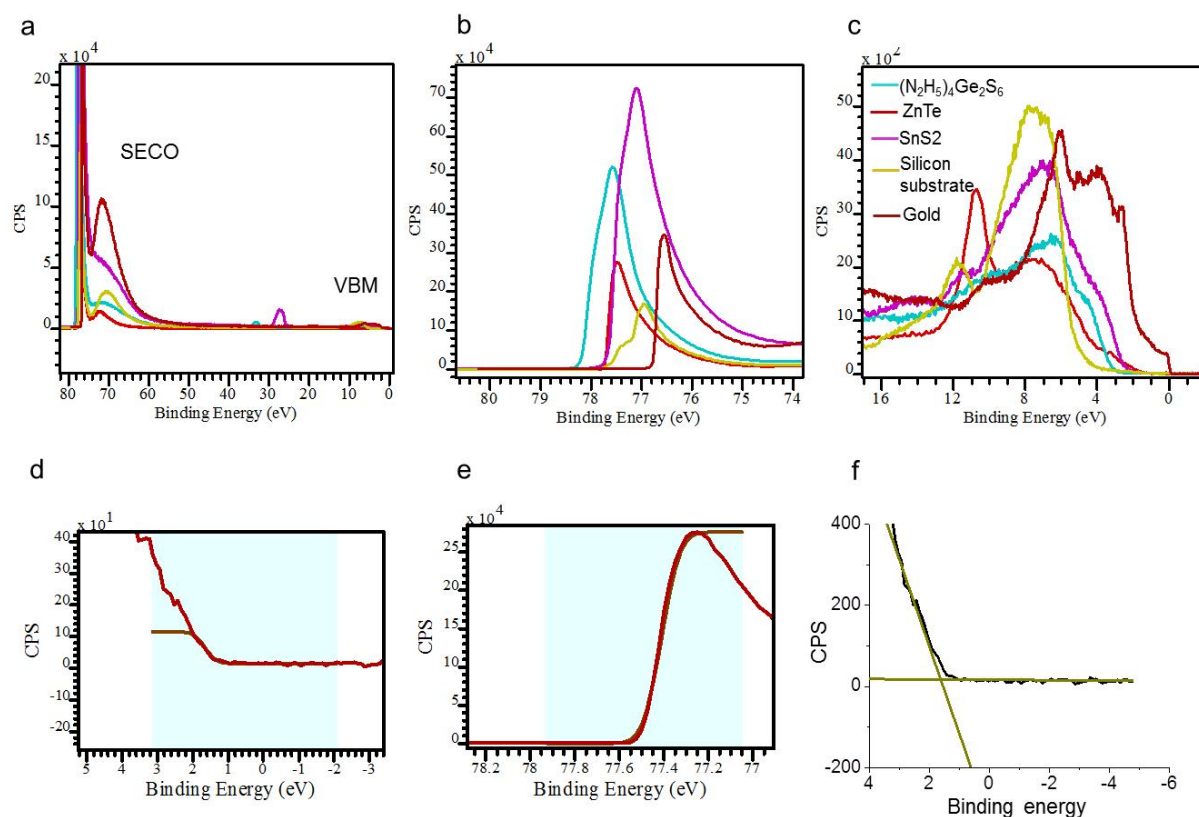


Figure S1 UPS spectra of the matrix materials and silicon substrate. **a**, The overview spectra. **b**, SECO region. **c**, VBM region. All labels for **a-c** included in **c**. **d-e**, Heaviside step function is used to fit the VBM and SECO region respectively of ZnTe. **f**, Intersection of the tangent to the low binding energy edge with the baseline (alternative determination of VBM). Both methods are consistent. The binding energy scale is relative to the Fermi level of gold.

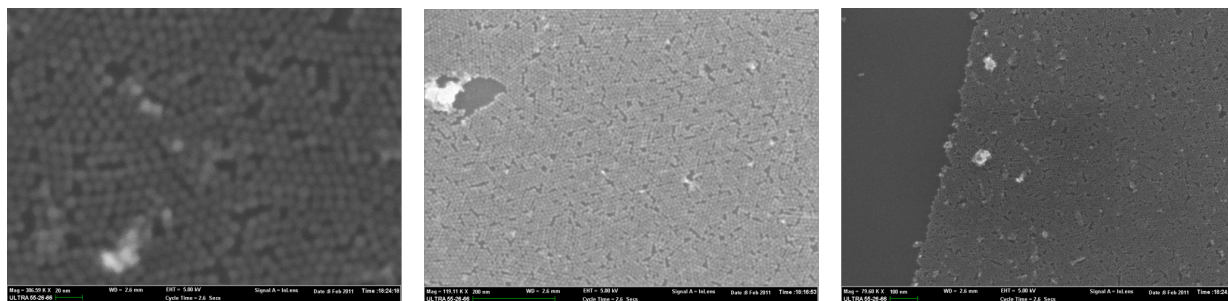


Figure S2 SEM images of a monolayer of PbSe-in-GeS₂ nanocomposite

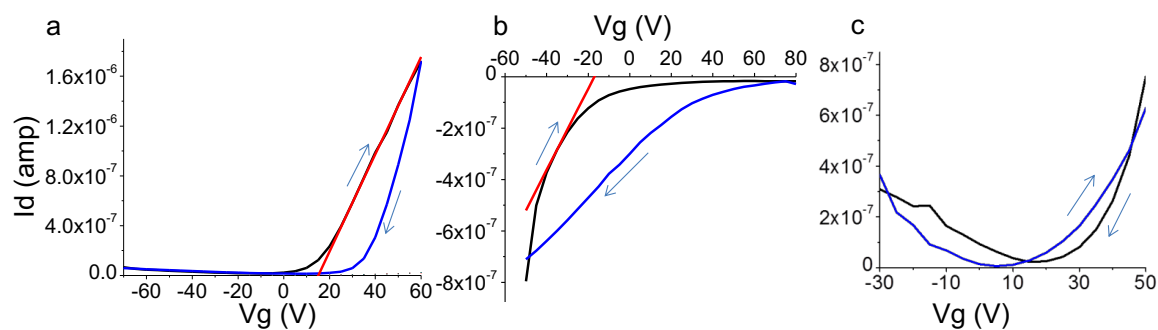


Figure S3 Transfer characteristics of PbSe nanocomposite TFTs. Calculation of linear regime mobilities is shown. **a**, PbSe-in-SnS₂ (V_d is 0.5V, slope of the tangent line is 3.9×10^{-8} S, calculated electron mobility is $0.49 \text{ cm}^2 \text{ V}^{-1} \text{ s}^{-1}$) **b**, PbSe-in-ZnTe. (V_d is -4V, slope of the tangent line is 1.58×10^{-8} S, calculated hole mobility is $0.026 \text{ cm}^2 \text{ V}^{-1} \text{ s}^{-1}$) **c**, PbSe-in-(N₂H₅)₄Ge₂S₆ (V_d is 10V, calculated electron and hole mobilities are 0.007 and $0.002 \text{ cm}^2 \text{ V}^{-1} \text{ s}^{-1}$, respectively). Black and blue data set represent the forward and reverse scans.

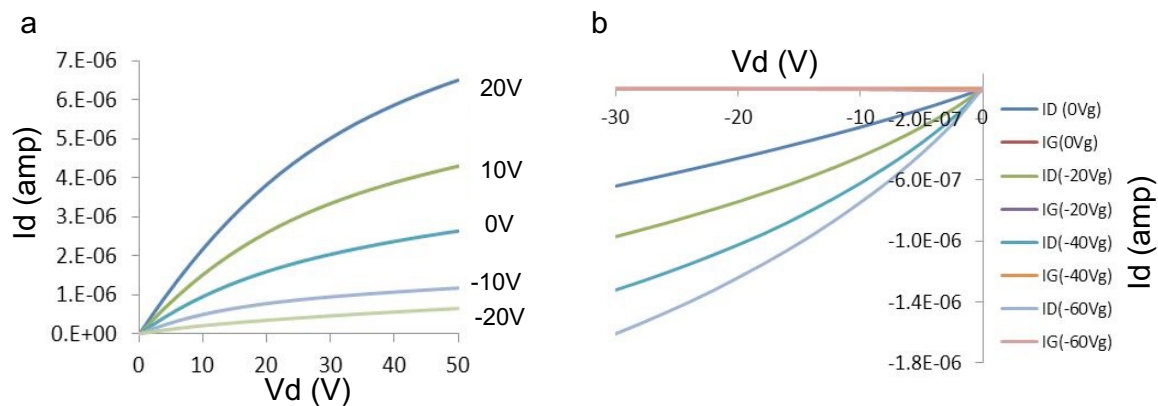


Figure S4 Output characteristics for PbSe nanocomposite TFTs with physically adhered indium dots as electrodes. a, PbSe-in-SnS₂. b, PbSe-in-ZnTe.

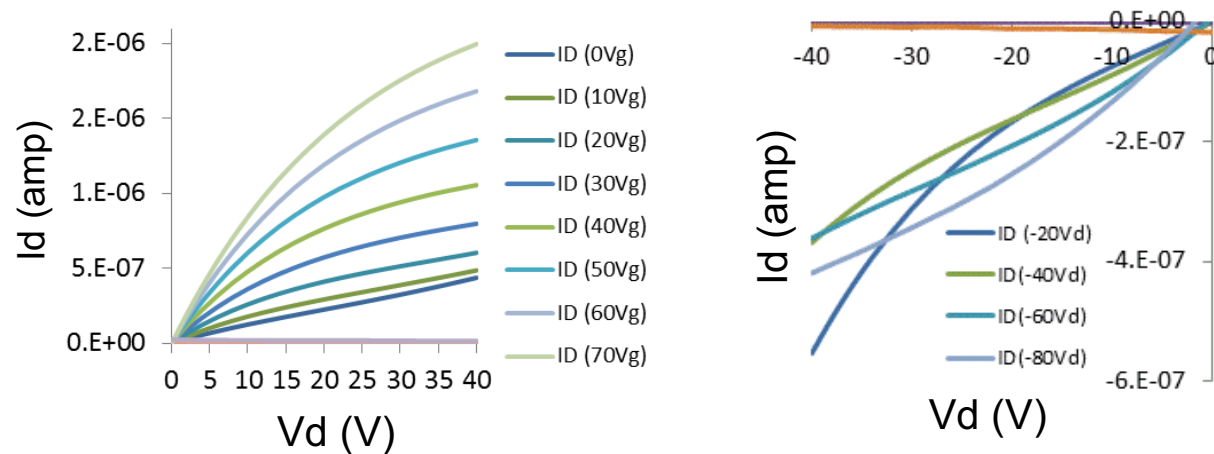


Figure S5 Output characteristics of TFTs with PbSe-GeS₂ nanocomposite channel layers.

The nanocomposite is synthesized by thermal annealing of PbSe-in-(N₂H₅)₄Ge₂S₆.

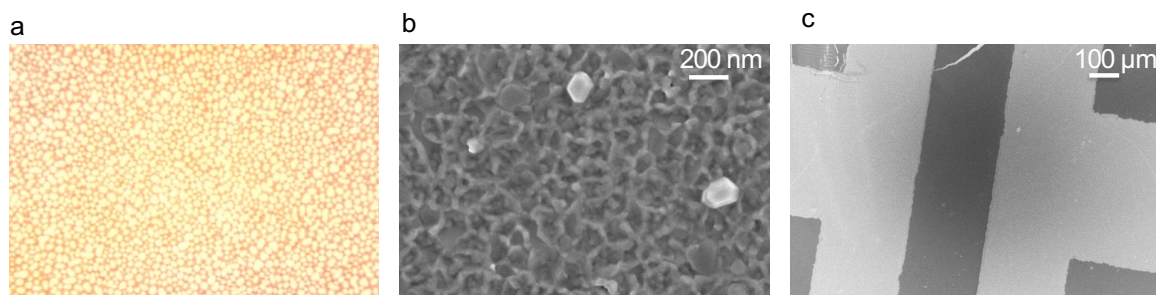


Figure S6 Processing of source/drain contacts of TFT devices: Indium metal evaporation (microscopic images). **a** Metal film morphology as discontinuous droplets due to high surface energy of indium. Indium film evaporated (SEM images). **b,c** SEM images of continuous films of indium. Composite of indium/gold is used as the adhesive thin-film material to attach indium onto SiO₂ substrates.

References

- (1) Yu, W. W.; Falkner, J. C.; Shih, B. S.; Colvin, V. L. Preparation and Characterization of Monodisperse PbSe Semiconductor Nanocrystals in a Noncoordinating Solvent. *Chem. Mater.* **2004**, *35*, 3318–3322.
- (2) Sharma, R.; Sawvel, A. M.; Barton, B.; Dong, A.; Buonsanti, R.; Llordes, A.; Schaible, E.; Axnanda, S.; Liu, Z.; Urban, J. J.; *et al.* Nanocrystal Superlattice Embedded within an Inorganic Semiconducting Matrix by in Situ Ligand Exchange: Fabrication and Morphology. *Chem. Mater.* **2015**, *27*, 2755–2758.